

Article type: Research Article

Temperature-Responsive 4D Liquid Crystal Microactuators Fabricated by Direct Laser Writing by Two-Photon Polymerization

Marc del Pozo, Dr. Colm Delaney, Dr. ir. Marina Pilz da Cunha, Dr. Michael G. Debije, Dr. Larisa Florea* and Prof. dr. Albert P. H. J. Schenning*

M. del Pozo, Dr. Marina Pilz da Cunha, Dr. M. G. Debije, and Prof. dr. A. P. H. J. Schenning
Laboratory for Stimuli-responsive Functional Materials & Devices (SFD), Department of
Chemical Engineering and Chemistry, Eindhoven University of Technology (TU/e), Groene
Loper 3, 5600 MB Eindhoven, The Netherlands.

*E-mail: a.p.h.j.schenning@tue.nl

Prof. dr. A.P.H.J. Schenning

Institute for Complex Molecular Systems (ICMS), Eindhoven University of Technology, Groene
Loper 3, 5600 MB Eindhoven, The Netherlands

Dr. C. Delaney and Dr. L. Florea

School of Chemistry and AMBER, the SFI Research Centre for Advanced Materials and
BioEngineering Research, Trinity College Dublin, The University of Dublin, College Green,
Dublin 2, Ireland

*Email: floreal@tcd.ie

Keywords: responsive microstructures, two-photon polymerization, direct laser writing, liquid
crystals, four-dimensional printing, microrobots

Over the past decade, progress in direct laser writing by two-photon polymerization (DLW-TPP) of stimuli-responsive materials has made considerable inroads into the realization of micro-actuators. With the focus on performing complex tasks such as walking, grasping, or delivering drugs, these actuators require a controlled pre-programmed actuation. Liquid crystalline micro-actuators enable such programmed movement when the mesogenic alignment can be successfully controlled. To date, this has necessitated low crosslink density networks, which are not readily conducive to the fabrication of three-dimensional (3D) geometries. Herein, we report a liquid crystalline photoresist, resulting in a highly crosslinked network, that permits fabrication of four-dimensional (4D) micro-actuators having a highly crosslinked network in which the molecular alignment is determined by the alignment layers in the cell construct. In addition to controllable deformation of the micro-actuators, they also display a characteristic and unique polarization color that can be used for both identification and reporting in real time, enabling their integration into sensing and anti-anticounterfeiting microdevices.

1. Introduction

Additive manufacturing of stimuli-responsive materials,^[1–5] referred to as four-dimensional (4D) printing, has found exciting application in the generation of micro-actuators.^[3,6–14] Direct laser writing by two-photon polymerization (DLW-TPP), in particular, has proven suitable for inducing locally selective polymerization in various stimuli-responsive materials.^[3,6,9,10,15–19] This technique offers outstanding resolution and a high degree of freedom in structural design,^[9,20,21] which has been used to generate micro-actuators which can perform advanced tasks such as walking, grasping, swimming, and delivering drugs among others.^[6,8,10,15,17,22–24] Among the available stimuli-responsive materials, liquid crystals (LC) have attracted special attention for the fabrication of micro-actuators *via* DLW-TPP as they can deliver rapid, reversible, pre-programmed anisotropic shape deformations in both dry and wet environments.^[6,8,30,17,18,23,25–29] In an LC-based micro-actuator, control over the mesogenic alignment is key to pre-programming the actuation of the microstructure.^[31–33] To truly exploit the potential of highly functional three-dimensional (3D) liquid crystalline micro-actuators, we must first improve our understanding of the effect fabrication method and structure geometry play in mesogens alignment, and consequently, in actuator response.

This work reports a LC-photoresist suitable for DLW-TPP fabrication of temperature responsive 4D micro-actuators with a highly crosslinked network. We present a series of uniaxially aligned 3D structures which demonstrate the mesogenic alignment is dictated by the alignment layer in the cell construct and not by the DLW-TPP parameters, allowing for the fabrication of microstructures with pre-programmed shape changes. Furthermore, owed to monolithic alignment, a characteristic and unique polarization color is observed that can be used to identify and differentiate the structures. The fabricated 3D microstructures are responsive to temperature variations which trigger anisotropic shape changes of different

amplitudes, depending on the structure's geometry. We present a full structural and optical characterization of the 3D constructs at different temperatures. The results present the advantages and limitations of using densely crosslinked liquid crystalline networks to fabricate micro-actuators *via* DLW-TPP.

2. Results and Discussion

2.1. LC-photoresist

The LC-photoresist used in this work consists of two classes of reactive mesogens: **1-3** are difunctional mesogenic acrylates (58.4 mol%) acting as crosslinkers, and **4** is a monofunctional mesogenic acrylate (40.0 mol%) that brings flexibility to the network, **Figure 1a**. This LC mixture has an isotropic to nematic temperature ($T_{I/N}$) at $\sim 100^\circ\text{C}$ with the nematic LC phase at room temperature without any signs of crystallization after at least 8h (**Figure S1**). To enable two-photon polymerization (TPP), 1.3 mol% of **5**, a photoinitiator, was added. The photoinitiator chosen has been employed previously to induce DLW-TPP in acrylate-based resists.^[17,24,34–36]

By fabricating a polymer film using the LC-photoresist, the glass transition temperature (T_g) of the material was found to be $\sim 69^\circ\text{C}$ and its degradation temperature ($T_{\text{degradation}}$) $\sim 363^\circ\text{C}$, **Figure S2**. Above T_g , the network is in its softer, rubbery state,^[37] and a higher temperature response is expected. In contrast, $T_{\text{degradation}}$ represents the temperature at which the polymer starts to irreversibly degrade and so actuation of the structures was conducted well below this temperature.

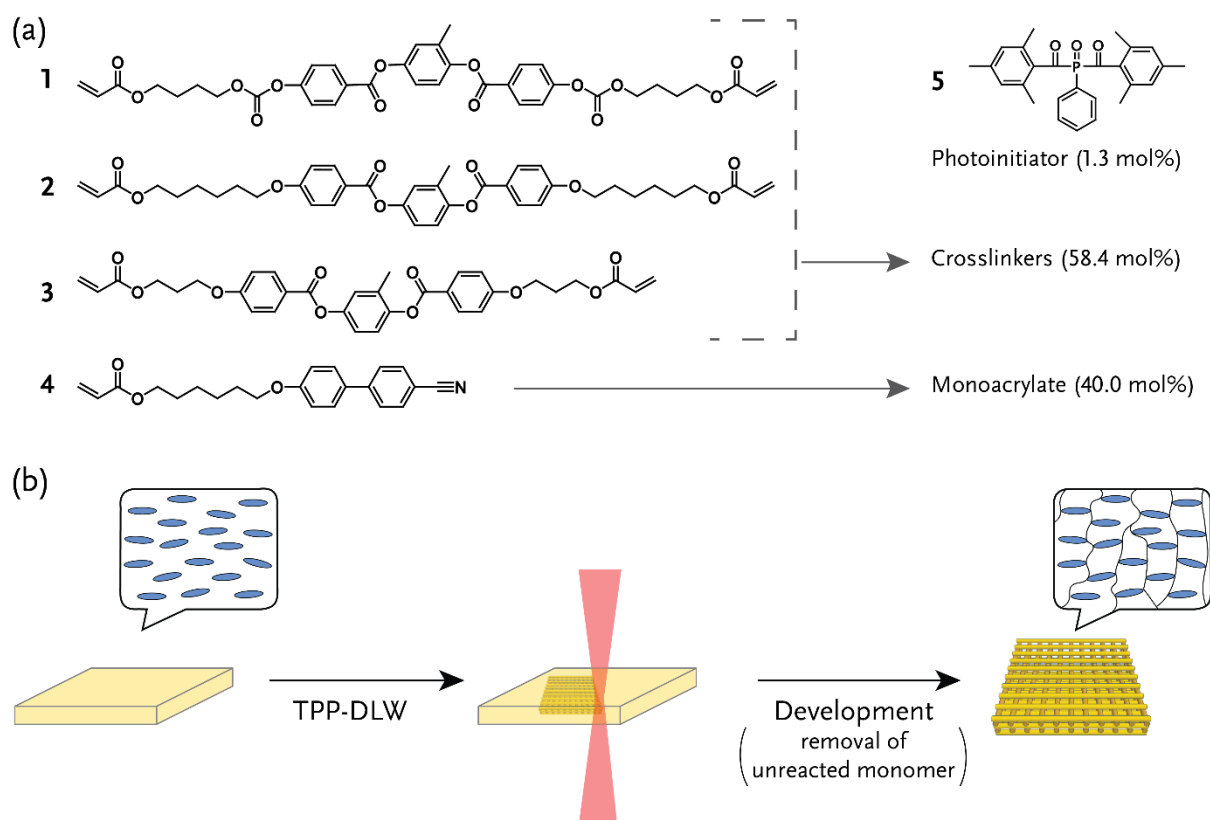


Figure 1. (a) Overview of reactive mesogens and photoinitiator used to prepare the LC-photoresist. (b) Schematic representation of the fabrication process for temperature responsive uniaxially aligned 3D microstructures. The blue rods represent the mesogens, which align along the longitudinal axis of the cell construct.

2.2. Fabrication of Uniaxially Aligned 3D Microstructures

The fabrication process of uniaxially aligned 3D microstructures *via* DLW-TPP comprises several steps which are depicted in **Figure 1b**. Firstly, a cell (consisting of two glass plates held together by a 50 μm double-sided tape) prepared with alignment layers was filled with the LC-photoresist at 105 $^{\circ}\text{C}$ using capillary forces. After filling, the cell was slowly cooled to room temperature, where the mixture exists in the more ordered nematic phase. The DLW-TPP process was then carried out to create 3D structures, examples of which are shown in **Figure S3** (hexagonal plates of 3 μm height and 20 μm width). The optimal writing speed was found

to be 10 mm s^{-1} , with laser ($\lambda = 780 \text{ nm}$) powers from 20-25 mW. After completion, a development step took place, consisting of submerging the cell in warm isopropanol to dissolve unreacted monomers. Fabrication of the structures was started $-0.5 \text{ }\mu\text{m}$ from the glass/photoresist interface to improve the adhesion of the structures to the substrate. This served to avoid delamination, and any minor mismatch between the computer aided design (CAD) and the structure's height can be attributed to this offset. After development, complete polymerization was confirmed *via* confocal Raman spectroscopy by verifying the disappearance of the peak corresponding to the double-bond stretch of the acrylate group at 1635 cm^{-1} and 1725 cm^{-1} (**Figure S4**).

The dimensions and shape of the hexagonal plates were characterized *via* scanning electron microscopy (SEM), **Figure 2a**. The structures consist of an average $18.5 \pm 0.3 \text{ }\mu\text{m} \times 19.4 \pm 0.6 \text{ }\mu\text{m}$ hexagons with an average height of $2.4 \pm 0.2 \text{ }\mu\text{m}$. One dimension of the plates was remarkably close to the CAD design while the other dimension was $\sim 8\%$ shorter. 5-10% polymerization shrinkage is normal in acrylic samples,^[38] and it occurs anisotropically in uniaxially aligned LC samples,^[39] with the majority of the shrinkage along the axis parallel to the alignment, as was observed here. Further shrinkage could also be attributed to the removal of unreacted monomer from the network during the development step; however, we expect this to be minimal due to the high crosslink density of the network and the complete polymerization as verified by confocal Raman spectroscopy. Horizontal lines depicting the laser writing path are clearly visible in the electron micrograph: the lines effectively exhibit the polymerization voxel with a width of $\sim 245 \text{ nm}$ when DLW was performed at a 10 mm s^{-1} with 25 mW laser power. Overall, the plates showed a good resemblance to the CAD design, indicating a good performance of the LC-photoresist with the DLW-TPP process.

The influence of the laser path during fabrication on the mesogenic alignment was investigated in the hexagonal plates. Three different plates were explored, **Figure 2b**. The first plate was fabricated by scanning the laser parallel to the alignment (0°). For the second and third samples, the scanning paths were rotated 45° and 90° to the alignment, respectively. In all three cases, the fabricated plates showed similar dimensions and geometries (**Figure 2b** and **Table S1**), indicating that the path chosen to fabricate the plate did not have a significant influence on the resulting size. The mesogenic alignment was characterized by polarized optical microscopy. Regardless of the laser path chosen, all plates appeared darker when the cell alignment was parallel to the polarizer or analyzer and showed a stronger blue polarization color when aligned at 45° to the polarizer or analyzer due to the anisotropic optical property of LCs (*vide infra*). Such dark–bright states are associated with the presence of uniaxial alignment.^[33,40,41] Thus, the mesogenic alignment of these microstructures is determined by the alignment layer in the cell construct and not by the fabrication parameters or the scanning direction of the laser. This allows for facile pre-programmed determination of the alignment in the structures by selection of appropriate alignment layers prior to fabrication.

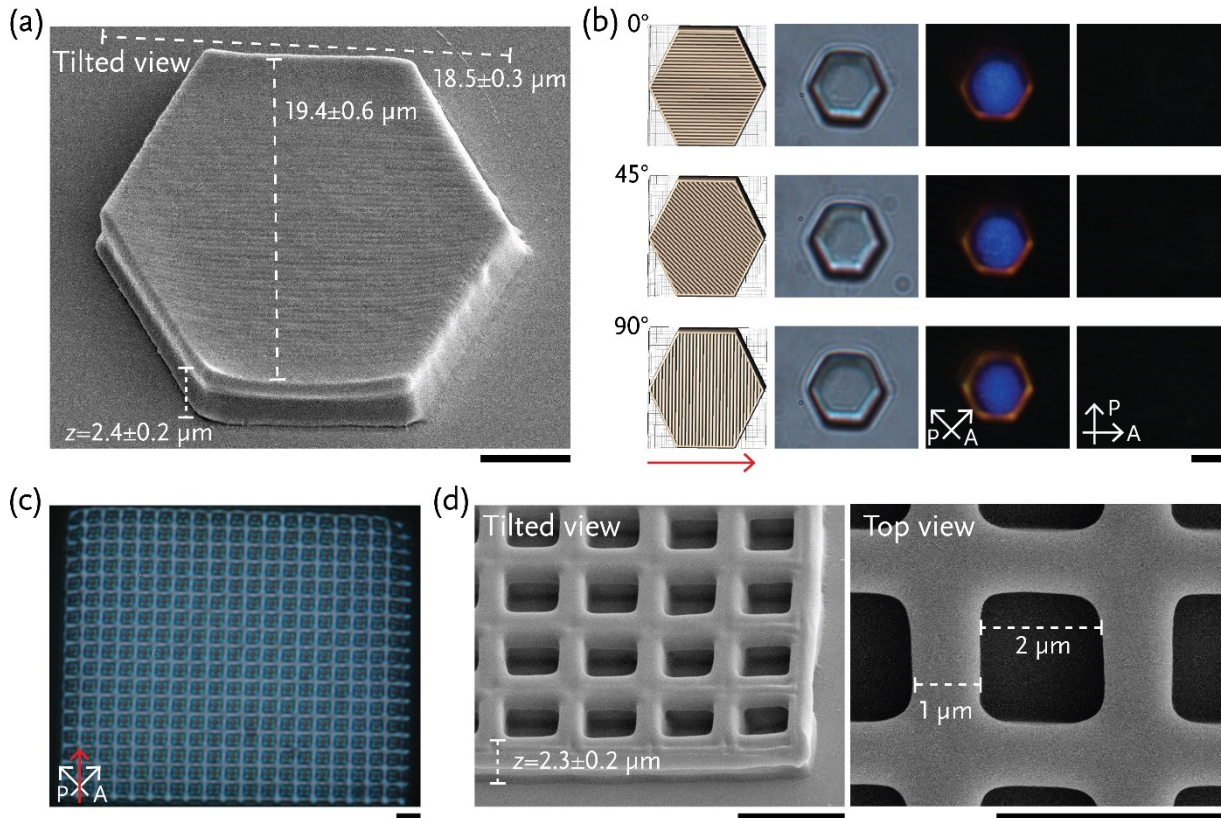


Figure 2. (a) Electron micrograph of a hexagonal plate; the CAD design is available in **Figure S3**. The sample was tilted at 40° to visualize and characterize its 3D dimensions. (b) On the left, the CAD designs of hexagonal plates of $9 \mu\text{m} \times 9 \mu\text{m} \times 4 \mu\text{m}$ in which the predetermined path of the laser is indicated in the drawings. The rectilinear paths are 0° , 45° , or 90° shifted with respect to the alignment of the mesogens in the cell, which is indicated by the red arrow. On the right, a series of optical micrographs of the fabricated hexagonal plates without and with crossed polarizers. (c) Polarized optical micrograph of the grid; the CAD design available in **Figure S3**. In (b) and (c) the white arrows indicate the direction of the polarizer (P) and analyzer (A). (d) Electron micrographs of the grid shown in (c). The micrograph offering a tilted view was taken with the sample tilted 40° . All scale bars represent $4 \mu\text{m}$. Error bars represent standard deviations for $N = 3$ measurements.

A grid in which the horizontal lines were fabricated with scans parallel to the alignment while the vertical lines were fabricated with scans perpendicular to the alignment layer direction was then fabricated (**Figure 2c-d** and **Figure S3**). Both vertical and horizontal lines showed the

same monolithic alignment, reinforcing the finding that the scanning direction does not disturb the alignment in the cell. The grid had uniaxially aligned lines of $\sim 1 \mu\text{m}$ in width with a periodicity of $\sim 2 \mu\text{m}$, and a height of $2.3 \pm 0.2 \mu\text{m}$.

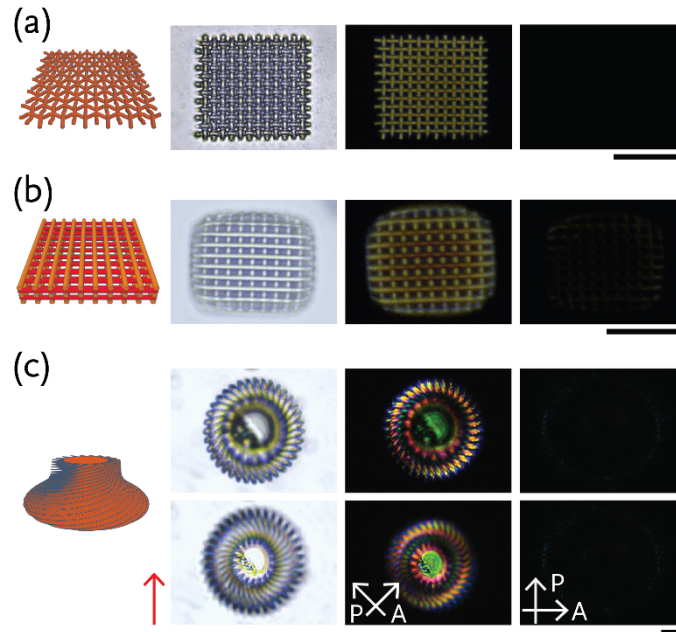


Figure 3. Uniaxial aligned 3D microstructures. (a) An interwoven fabric structure, (b) a woodpile, and (c) a spiral disk. On the left, the CAD designs. On the right, optical micrographs of the fabricated structures without and with crossed polarizers. For (c) the top row shows the spiral disk when the focus is located at the bottom of the structure and the bottom row when it is placed on the top of it. The red arrow indicates the direction of the alignment. The white arrows indicate the direction of the polarizer (P) and analyzer (A). All scale bars represent $20 \mu\text{m}$.

The potential of the presented LC-photoresist with the DLW-TPP process was explored by fabricating more complex geometries, **Figure 3**. To this end, we fabricated an interwoven fabric, a woodpile, and a spiral disk. The interwoven fabric embodies a flat geometry that has interconnected features. The woodpile shows the possibility of fabricating a 3D photonic crystal,

and the spiral disk demonstrates the capability of making structures that constantly change dimensions in all three planes. In all three cases, the structures showed good fidelity to the CAD design. Upon investigating the molecular alignment by polarized optical microscopy, we verified that the microstructures exhibited monolithic alignment. Furthermore, the microstructures displayed distinct polarization colors: the interwoven fabric and woodpile structures displayed a yellow color, while the spiral disk exhibited a range of different colors. These colors arise from the anisotropic optical property of LCs, defined as the difference between the extraordinary (n_e) and ordinary (n_o) refractive indices, also known as birefringence ($\Delta n = n_e - n_o$).^[33,40] When light travels through a uniaxially aligned LC sample with a specific thickness (d), it encounters an optical path difference ($OPD = d \Delta n$) between transmitted extraordinary and ordinary rays that results in a polarization color when observed between crossed polarizers. Thus, the colors are dependent on the structure's height and geometry. This supports the presence of multiple colors observed for the spiral disk, and one single color in the “flat” interwoven fabric structure, for example. This unique and characteristic polarization color facilitates the object's identification, a characteristic much desired in the micro realm.^[17,42]

2.3. Temperature Response

The temperature response of a row of hexagonal plates ($18.5 \pm 0.3 \mu\text{m} \times 19.4 \pm 0.6 \mu\text{m} \times 4.1 \pm 0.1 \mu\text{m}$) was characterized using an optical profiling system. Upon heating from $20 \text{ }^\circ\text{C}$ to $220 \text{ }^\circ\text{C}$, the plates showed an anisotropic shape change, contracting along the side parallel to the alignment direction (x) and expanding along the perpendicular side (y), with an increase in height (z); see **Figure 4a**. The anisotropic temperature response observed in the x and y directions is characteristic of uniaxially aligned networks. Such response comes from the increased molecular disorder induced by temperature that results in a contraction in the

direction parallel to the alignment and in an expansion perpendicular to it.^[6,30,33] A more detailed analysis of the temperature induced change of the plates' dimensions revealed that temperature response starts above 60 °C, **Figure 4b**. This onset temperature is close to the T_g , ~69 °C, of the network. Above the T_g the network is less stiff, resulting in the observed anisotropic shape change. At 220 °C, a contraction of $-4.2\pm 0.1\%$ was observed in the x direction, with an expansion of $4.3\pm 0.1\%$ and $10.2\pm 0.1\%$, seen in the y and z orientations, respectively, compared to their dimensions at 20 °C. The larger shape change observed in the z direction (~10%) with respect to the other orientations (~4%) could be attributed to the strong adherence of these structures to the glass substrate. We have previously characterized the swelling of micron sized structures fabricated using DLW-TPP.^[19] Adhesion can play significant role in limitation of axial swelling, thereby focusing the possible swelling into the direction perpendicular to the substrate. Here a similar limitation could be occurring, explaining the bigger shape change in the z orientation. Additionally, the height changes between 30 °C to 220 °C over ten heating/cooling cycles were measured, and the results displayed in **Figure 4c**. The data show a reversible shape change with no indication of fatigue despite the actuation being at elevated temperatures.

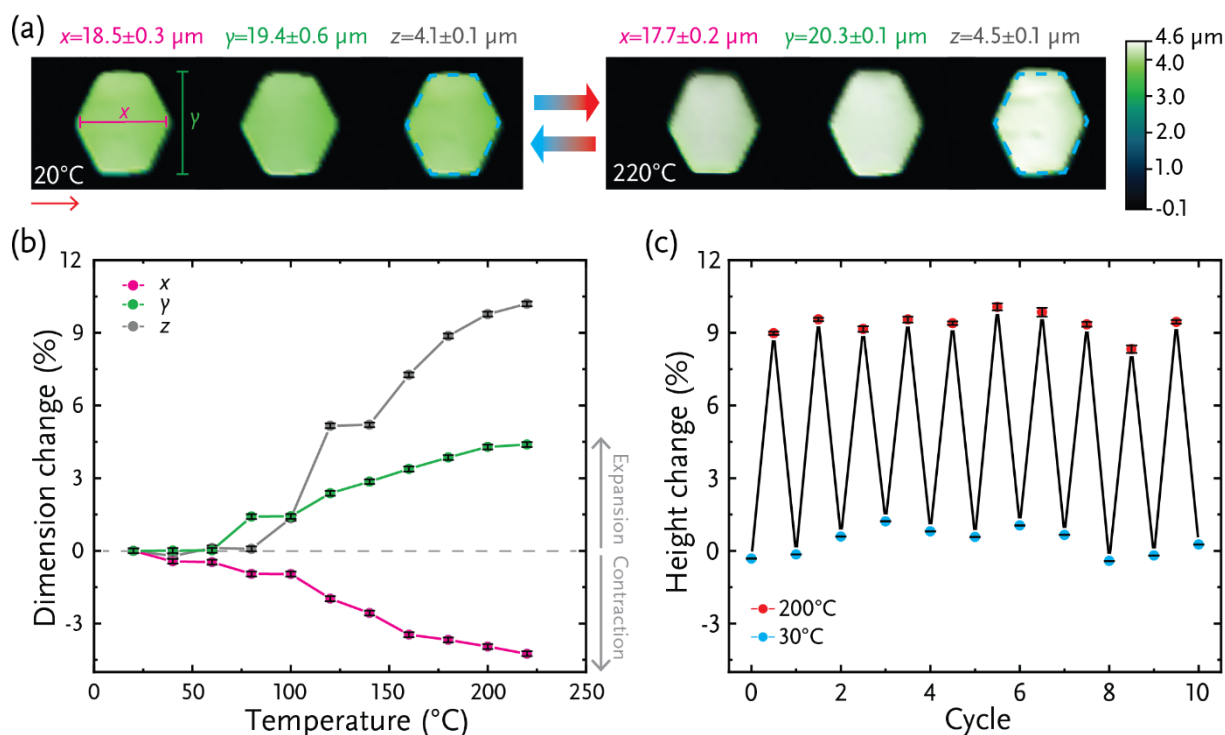


Figure 4. (a) 3D profiles of an array of hexagonal plates at 20°C and 220°C. The red arrow indicates the direction of the alignment of the mesogens. The blue dashed lines represent the contour of a plate at 20°C. (b) Dimension change of the plates over a range of different temperatures. The dimensions x and y are indicated in (a). (c) Height variation of the hexagonal plates over ten heating and cooling cycles, from 30°C to 200°C. For both (b) and (c), the fractional change is determined by comparing the current dimension of the plate with its value at 20°C. For all measurements, the temperature was held for 5 min before recording the dimension. Error bars represent standard deviations for $N = 3$ measurements.

Finally, the temperature responses of a woodpile and a spiral disk were also investigated. In this case, the woodpile structure studied was composed of more stacks than depicted in **Figure 3** and therefore its birefringence color appeared blue instead of yellow, **Figure 5**. Upon heating to 200°C, the structures showed an anisotropic shape change like those observed in the hexagonal plates (**Figure 4**). The woodpile reduced its dimensions by 7% parallel to the mesogenic alignment and increased by 6.5% perpendicular to it. Remarkably, the spiral disk

expanded around by 26% perpendicular to the alignment while it contracted only -5.5% in the parallel direction. When cooling to 30°C, the structures recovered their initial shapes and dimensions. The enhanced performance of both structures in the xy -plane, which for the spiral disk is also significantly asymmetrical, in comparison with the plates, can be explained by the difference in geometries that bring higher degrees of freedom when actuating, which can directly affect the actuation of the microstructure. It has been shown before that by changing the geometry^[23] or by making the structure free-standing,^[43,44] larger actuation could be obtained. However, this is the first time that non-freestanding structures made from the same LC network show different percentages of shape changes when their response is triggered by an external stimulus; this highlights the importance of choosing the optimal shape of the micro-actuator in addition to the suitability of the material. Furthermore, temperature also had an influence on the polarization color of the structures. Upon incremental changes in temperature, both the structure thickness, d , and birefringence, Δn change accordingly. These changes are matched with a change OPD, which is responsible for the polarization color (*vide supra*).^[33,40] As a result, this inherent color can act as both an identifier and sensor for the microstructures,.

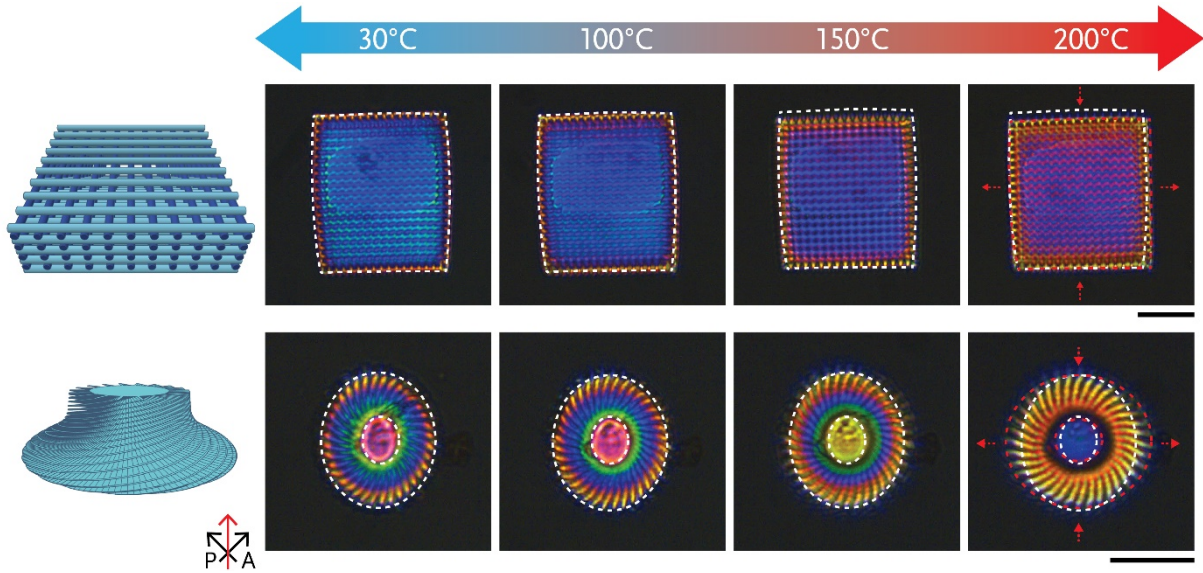


Figure 5. Temperature response of the 3D woodpile (top) and spiral disk (bottom) microstructures. From left to right: the CAD design and sets of crossed polarized optical micrographs recorded at different temperatures. The white and red dashed lines illustrate the contour of the structure at 30°C and 200°C, respectively. The red dashed arrows mark the direction of the shape change that occurs upon heating. The black arrows indicate the direction of the polarizer (P) and analyzer (A). The solid red arrow represents the direction of the alignment. The scale bars represent 20 μm .

3. Conclusion

Through the development of a LC-photoresist, high-resolution 4D micro-actuators were fabricated *via* direct laser writing by two-photon polymerization. The mesogenic alignment of the structures was dictated by the alignment layers in the cell construct and was unperturbed by structure design or writing direction. As a result, a series of uniaxially aligned LC 3D microstructures were successfully fabricated, displaying good fidelity to the CAD design. The structures showed reversible, anisotropic shape changes triggered by temperature, which resulted in expansions from 10-26% at 200 °C, and were dictated by the structure geometry. The anisotropic shape change is attributed to the increased disorder that the mesogens undergo

upon a temperature increase and can be easily controlled by modulating the direction of the mesogenic alignment. Furthermore, owed to the monolithic alignment, the structures have unique and responsive polarization colors enabling differentiation between structures, and self-reporting of their status. The LC-photoresist presented is an excellent candidate for fabrication of responsive micro-actuators with pre-programmed deformations and in-built color sensors that allow identification and *in situ* readability of their performance.

4. Methods

Materials and Reagents: 2-methyl-1,4-phenylene bis(4-(((4-(acryloyloxy)butoxy)carbonyloxy)benzoate) (**1**) was purchased from BASF. 1,4-di(4-(6-acryloyloxyhexyloxy)benzoyloxy)-2-methylbenzene (**2**), 1,4-di(4-(3-acryloyloxypropyloxy)benzoyloxy)-2-methylbenzene (**3**), and 4-(4-(6-acryloyloxyhexyloxy)benzoyloxy)benzotrile (**4**) were supplied by Merck. The photoinitiator bis(2,4,6-trimethylbenzoyl)phenylphosphine oxide was purchased from Ciba Specialty and the thermal inhibitor 2-tert-butylbenzene-1,4-diol from Sigma-Aldrich. The polyamide AL 1051 was obtained from JSR Micro. All solvents were purchased from Biosolve.

LC photoresist Preparation and Characterization: The LC-photoresist consisted of 33.3 mol% **1**, 11.7 mol% **2**, 13.4 mol% **3**, 40.0 mol% **4**, 1.3 mol% photoinitiator. To avoid temperature-induced polymerization during the filling of the cell, a small quantity of polymerization inhibitor, 0.3 mol%, was incorporated. As a result, the LC photoresist can be maintained at 105°C for up to 8h without polymerizing (**Figure S1**). All components were dissolved in dichloromethane. The solvent was removed at 60 °C overnight under magnetic stirring. Characterization of the resulting LC mixture can be found in the *Supplementary Information*.

Cell Preparation: High-precision microscope cover glasses ($22 \times 22 \text{ mm}^2$, thickness $170 \pm 5 \text{ }\mu\text{m}$; from Marienfeld) were cleaned by sonication for 20 min in acetone and subsequently treated in a UV-ozone photoreactor (Ultra Violet Products, PR-100) for 20 min to activate the surface. Polyamide AL 1051 was immediately spin coated on the glass (step 1: 800 rpm for 5 s; step 2: 5000 rpm for 40s; both with an acceleration of 500 rpm s^{-1}) followed by a curing step of 180 min at $180 \text{ }^\circ\text{C}$. The polyimide layer was then uniaxially rubbed with a velvet cloth, and the cell assembly made using a $50 \text{ }\mu\text{m}$ thick double adhesive tape spacer in which the rubbed polyimide layer, acting as an alignment layers, were on the inside of the cell.

Computer Design of the Structures: All structures were fabricated based on a computer aided design. The designs of the hexagonal plates, grids, and woodpiles were custom made by the authors using the website www.tinkercad.com. The spiral disk and the fabric-like structure were adapted from files licensed under the Creative Commons Attribution 4.0 International license and available at www.thingiverse.com. The files were modified using DeScribe 2.4.4 software to choose the slicing ($0.2\text{--}0.5 \text{ }\mu\text{m}$) and hatching ($0.2 \text{ }\mu\text{m}$) values.

Direct Laser Writing: First, the cell assembly was filled using capillary action with the LC-photoresist in its isotropic phase at 105°C . After filling, the temperature was slowly lowered to room temperature. Below the T_{IN} , the molecules aligned parallel to the rubbing direction,^[33] which in this case resulted in a uniaxial alignment, confirmed *in situ* by observing the cell between crossed polarizers. After verification of the alignment, localized TTP was performed in a commercial DLW workstation (Photonic Professional, Nanoscribe GmbH) equipped with a 170 mW femtosecond solid-state laser ($\lambda = 780 \text{ nm}$) that delivers 120 fs pulses with an $80 \text{ MHz} \pm 1 \text{ MHz}$ repetition rate. At a power scaling of 1, the average laser output is 50 mW. The laser beam was focused with a $63\times$ oil objective ($\text{NA} = 1.4$; $\text{WD} = 190 \text{ }\mu\text{m}$; Zeiss; Plan Apochromat) into the filled cell. The sample movement was controlled by a piezo translation

stage in the z-axis and by a galvo stage in the x- and y-axes. The fabrication of the 3D microstructures was performed with scan speeds of 10 mm s^{-1} and laser powers between 20–25 mW, depending on the structure's geometry, hatching, and slicing values. The fabrication started $0.5 \text{ }\mu\text{m}$ below the automatically detected glass/photonic photoresist interface. Finally, the cell was submerged in warm isopropanol to dissolve the unreacted monomer. The cell was then carefully opened, and the glass rinsed with isopropanol and then air-dried.

Structure Characterization: Electron micrographs were recorded using a Quanta FEG 3D SEM in secondary electron mode, beam current of 5 kV. Prior to imaging, the structures were sputtered coated with an Au-Pd layer. Optical micrographs were recorded on a Leica DM2700 M polarized optical microscope equipped with a Leica MC170 HD camera. All structures were visualized both in bright field and in transmission modes. The 3D profiles of the structures were obtained using an optical profiling system (S Neox 3D Optical profiler, equipped with a $\times 50$ objective). When characterizing the temperature response of the structures, both the microscope and the optical profiling system were equipped with a Linkam TMS 600 hot-stage.

Acknowledgements

M. del Pozo, M. G. Debije, and A. P. H. J. Schenning extend their gratitude towards our project partners in the DynAM project consortium (“Dynamic Materials for Additive Manufacturing”). The project is funded by the Dutch Research Council (NWO) in the framework of the Innovation Fund Chemistry, and from the Dutch Ministry of Economic Affairs and Climate Policy in the framework of the PPP allowance. This research received funding from the European Horizon 2020 Research and Innovation Programme (No. 899349 - 5D NanoPrinting) and Science Foundation Ireland (SFI) under grant number 12/RC/2278_P2. C Delaney acknowledges support from the Irish Research Council through the Government of

Ireland Postdoctoral Fellowship Scheme; Grant Number GOIPD/2020/484. The DLW-TPP fabrication and some of the imaging for this project was carried out at the Additive Research Laboratory (AR-Lab) and the Advanced Microscopy Laboratory (AML), Trinity College Dublin, Ireland. The AR-Lab and AML are SFI supported centers, part of the CRANN Institute and affiliated to the AMBER center. S.J.A. Houben and Y. Foelen are thanked for performing SEM imaging and thermogravimetric analysis (TGA), respectively. Finally, the authors are grateful to J.A.H.P. Sol for his insight on the design and style of the figures.

References

- [1] S. Nocentini, D. Martella, C. Parmeggiani, D. S. Wiersma, *Adv. Opt. Mater.* **2019**, *7*, 1900156.
- [2] J. del Barrio, C. Sánchez-Somolinos, *Adv. Opt. Mater.* **2019**, *7*, 1900598.
- [3] C. A. Spiegel, M. Hippler, A. Münchinger, M. Bastmeyer, C. Barner-Kowollik, M. Wegener, E. Blasco, *Adv. Funct. Mater.* **2020**, *30*, 1907615.
- [4] Y. Yang, X. Song, X. Li, Z. Chen, C. Zhou, Q. Zhou, Y. Chen, *Adv. Mater.* **2018**, *30*, 1706539.
- [5] S. Miao, N. Castro, M. Nowicki, L. Xia, H. Cui, X. Zhou, W. Zhu, S. jun Lee, K. Sarkar, G. Vozzi, Y. Tabata, J. Fisher, L. G. Zhang, *Mater. Today* **2017**, *20*, 577.
- [6] H. Zeng, P. Wasylczyk, C. Parmeggiani, D. Martella, M. Burrese, D. S. Wiersma, *Adv. Mater.* **2015**, *27*, 3883.
- [7] M. Hippler, E. Blasco, J. Qu, M. Tanaka, C. Barner-Kowollik, M. Wegener, M. Bastmeyer, *Nat. Commun.* **2019**, *10*, 232.
- [8] D. Martella, S. Nocentini, D. Nuzhdin, C. Parmeggiani, D. S. Wiersma, *Adv. Mater.* **2017**, *29*, 1704047.
- [9] A. K. Nguyen, R. J. Narayan, *Mater. Today* **2017**, *20*, 314.
- [10] D. Jin, Q. Chen, T. Y. Huang, J. Huang, L. Zhang, H. Duan, *Mater. Today* **2019**, *32*, 19.
- [11] Y. W. Lee, H. Ceylan, I. C. Yasa, U. Kilic, M. Sitti, *ACS Appl. Mater. Interfaces* **2021**, *13*, 12759.
- [12] C. Yang, B. Wu, J. Ruan, P. Zhao, L. Chen, D. Chen, F. Ye, *Adv. Mater.* **2021**, 2006361.
- [13] Q. Chen, P. Lv, J. Huang, T.-Y. Huang, H. Duan, *Research* **2021**, *2021*, 1.
- [14] M. Tabrizi, T. H. Ware, M. R. Shankar, *ACS Appl. Mater. Interfaces* **2019**, *11*, 28236.
- [15] M. Dong, X. Wang, X. Z. Chen, F. Mushtaq, S. Deng, C. Zhu, H. Torlakcik, A.

- Terzopoulou, X. H. Qin, X. Xiao, J. Puigmartí-Luis, H. Choi, A. P. Pêgo, Q. D. Shen, B. J. Nelson, S. Pané, *Adv. Funct. Mater.* **2020**, *30*, 1910323.
- [16] Y. Hu, Z. Wang, D. Jin, C. Zhang, R. Sun, Z. Li, K. Hu, J. Ni, Z. Cai, D. Pan, X. Wang, W. Zhu, J. Li, D. Wu, L. Zhang, J. Chu, *Adv. Funct. Mater.* **2020**, *30*, 1907377.
- [17] M. del Pozo, C. Delaney, C. W. M. Bastiaansen, D. Diamond, A. P. H. J. Schenning, L. Florea, *ACS Nano* **2020**, *14*, 9832.
- [18] C. C. Tartan, J. J. Sandford O'Neill, P. S. Salter, J. Aplinc, M. J. Booth, M. Ravnik, S. M. Morris, S. J. Elston, *Adv. Opt. Mater.* **2018**, *6*, 1800515.
- [19] A. Tudor, C. Delaney, H. Zhang, A. J. Thompson, V. F. Curto, G. Z. Yang, M. J. Higgins, D. Diamond, L. Florea, *Mater. Today* **2018**, *21*, 807.
- [20] F. Rajabasadi, L. Schwarz, M. Medina-Sánchez, O. G. Schmidt, *Prog. Mater. Sci.* **2021**, *120*, 100808.
- [21] G. Adam, A. Benouhiba, K. Rabenoroso, C. Clévy, D. J. Cappelleri, *Adv. Intell. Syst.* **2021**, *3*, 2000216.
- [22] L. Chen, Y. Dong, C.-Y. Tang, L. Zhong, W.-C. Law, G. C. P. Tsui, Y. Yang, X. Xie, *ACS Appl. Mater. Interfaces* **2019**, *11*, 19541.
- [23] S. Nocentini, D. Martella, C. Parmeggiani, S. Zanotto, D. S. Wiersma, *Adv. Opt. Mater.* **2018**, *6*, 1800167.
- [24] C. C. Tartan, P. S. Salter, T. D. Wilkinson, M. J. Booth, S. M. Morris, S. J. Elston, *RSC Adv.* **2017**, *7*, 507.
- [25] Y. Guo, H. Shamsavan, M. Sitti, *Adv. Mater.* **2020**, *32*, 2002753.
- [26] S. Zanotto, F. Sgrignuoli, S. Nocentini, D. Martella, C. Parmeggiani, D. S. Wiersma, *Appl. Phys. Lett.* **2019**, *114*, 201103.
- [27] S. Nocentini, F. Riboli, M. Burrese, D. Martella, C. Parmeggiani, D. S. Wiersma, *ACS*

- Photonics* **2018**, *5*, 3222.
- [28] V. S. R. Jampani, D. J. Mulder, K. R. De Sousa, A.-H. Gélébart, J. P. F. Lagerwall, A. P. H. J. Schenning, *Adv. Funct. Mater.* **2018**, *28*, 1801209.
- [29] H. Yoshida, C. H. Lee, Y. Matsuhisa, A. Fujii, M. Ozaki, *Adv. Mater.* **2007**, *19*, 1187.
- [30] M. del Pozo, J. A. H. P. Sol, A. P. H. J. Schenning, M. G. Debije, *Adv. Mater.* **2021**, 2104390.
- [31] L. T. de Haan, J. M. N. Verjans, D. J. Broer, C. W. M. Bastiaansen, A. P. H. J. Schenning, *J. Am. Chem. Soc.* **2014**, *136*, 10585.
- [32] L. T. de Haan, C. Sánchez-Somolinos, C. W. M. Bastiaansen, A. P. H. J. Schenning, D. J. Broer, *Angew. Chemie - Int. Ed.* **2012**, *51*, 12469.
- [33] D. Liu, D. J. Broer, *Langmuir* **2014**, *30*, 13499.
- [34] C. P. Jisha, K.-C. Hsu, Y. Lin, J.-H. Lin, C.-C. Jeng, R.-K. Lee, *Opt. Lett.* **2012**, *37*, 4931.
- [35] C. C. Tartan, P. S. Salter, M. J. Booth, S. M. Morris, S. J. Elston, *J. Appl. Phys.* **2016**, *119*, 183106.
- [36] K. J. J. Schafer, J. M. M. Hales, M. Balu, K. D. D. Belfield, E. W. W. Van Stryland, D. J. J. Hagan, *J. Photochem. Photobiol. A Chem.* **2004**, *162*, 497.
- [37] D. C. Hoekstra, P. P. M. Visser, S. J. A. Houben, J. Lub, M. G. Debije, A. P. H. J. Schenning, *J. Appl. Phys.* **2021**, *129*, 75101.
- [38] M. H. Bland, N. A. Peppas, *Biomaterials* **1996**, *17*, 1109.
- [39] R. A. M. Hikmet, B. H. Zwerver, D. J. Broer, *Polymer (Guildf)*. **1992**, *33*, 89.
- [40] Y. Guo, H. Shahsavan, M. Sitti, *Adv. Opt. Mater.* **2020**, *8*, 1902098.
- [41] H. Zeng, D. Martella, P. Wasylczyk, G. Cerretti, J.-C. C. G. Lavocat, C.-H. H. Ho, C. Parmeggiani, D. S. Wiersma, *Adv. Mater.* **2014**, *26*, 2319.
- [42] C. A. Koepele, M. Guix, C. Bi, G. Adam, D. J. Cappelleri, *Adv. Intell. Syst.* **2020**, *2*,

1900147.

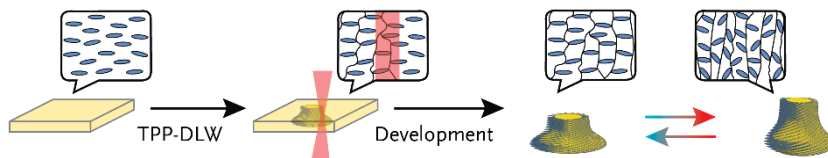
[43] S. Nocentini, D. Martella, C. Parmeggiani, D. Wiersma, *Materials (Basel)*. **2016**, *9*, 525.

[44] D. Martella, D. Antonioli, S. Nocentini, D. S. Wiersma, G. Galli, M. Laus, C. Parmeggiani, *RSC Adv*. **2017**, *7*, 19940.

Untethered micro-actuators are appealing to fields including medicine or microfluidics. However, their miniaturization is still challenging when specific geometries displaying pre-programmed deformations are desired. Here, a liquid crystalline photoresist with a high fraction of crosslinkers is reported and the structural and optical responses of several temperature responsive 3D constructs are studied.

M. del Pozo, C. Delaney, M. Pilz da Cunha, M. G. Debije, L. Florea* and A. P. H. J. Schenning*

Temperature-Responsive 4D Liquid Crystal Microactuators Fabricated by Direct Laser Writing by Two-Photon Polymerization



Supporting Information

Temperature-Responsive 4D Liquid Crystal Microactuators Fabricated by Direct Laser

Writing by Two-Photon Polymerization

Marc del Pozo, Dr. Colm Delaney, Dr. ir. Marina Pilz da Cunha, Dr. Michael G. Debije, Dr. Larisa Florea* and Prof. dr. Albert P. H. J. Schenning*

M. del Pozo, Dr. Marina Pilz da Cunha, Dr. M. G. Debije, and Prof. dr. A. P. H. J. Schenning
Laboratory for Stimuli-responsive Functional Materials & Devices (SFD), Department of
Chemical Engineering and Chemistry, Eindhoven University of Technology (TU/e), Groene
Loper 3, 5600 MB Eindhoven, The Netherlands.

*E-mail: a.p.h.j.schenning@tue.nl

Prof. dr. A.P.H.J. Schenning

Institute for Complex Molecular Systems (ICMS), Eindhoven University of Technology, Groene
Loper 3, 5600 MB Eindhoven, The Netherlands

Dr. C. Delaney and Dr. L. Florea

School of Chemistry and AMBER, the SFI Research Centre for Advanced Materials and
BioEngineering Research, Trinity College Dublin, The University of Dublin, College Green,
Dublin 2, Ireland

*Email: floreal@tcd.ie

Keywords: responsive microstructures, two-photon polymerization, direct laser writing, liquid
crystals, four-dimensional printing, microrobots

Methods

Cell Preparation: glasses ($3 \times 3 \text{ mm}^2$) were cleaned by sonication for 20 min in acetone and subsequently treated in a UV-ozone photoreactor (Ultra Violet Products, PR-100) for 20 min to activate the surface. Polyamide AL 1051 was immediately spin coated on the glass (step 1: 800 rpm for 5 s; step 2: 5000 rpm for 40s; both with an acceleration of 500 rpm s^{-1}) followed by a curing step of 180 min at $180 \text{ }^\circ\text{C}$. The polyimide layer was then uniaxially rubbed with a velvet cloth, and the cell assembly made using a $50 \text{ }\mu\text{m}$ thick double adhesive tape spacer in which the rubbed polyimide layer, acting as an alignment layers, were on the inside of the cell.

Liquid Crystalline Film Preparation: First, the cell assembly, prepared as described in the main text but using thicker glass slides, was filled by capillarity action with the liquid crystal (LC)-photoresist in its isotropic phase at $105 \text{ }^\circ\text{C}$. After filling, the temperature was slowly lowered to room temperature. Photo-copolymerization of the monomer mixture was performed at room temperature with an Exfo Omnicure S2000 light source in which 57% of the light intensity has a wavelength of 395-445 nm and 43% of 320-390 nm. The exposed sample was then left at $120 \text{ }^\circ\text{C}$ for 30 min to release any polymerization induced stresses. The cell was finally opened to obtain a free-standing film.

Characterization: Differential scanning calorimetry (DSC) was performed with a DSC Q2000 from TA Instruments with an aluminum hermetic crucible. All tests were conducted in a nitrogen environment. The temperature ranged between $-30 \text{ }^\circ\text{C}$ and $130 \text{ }^\circ\text{C}$ for the LC-photoresist and between $-50 \text{ }^\circ\text{C}$ and $230 \text{ }^\circ\text{C}$ for the LC-film, in both cases with heating and cooling rates of $5 \text{ }^\circ\text{C min}^{-1}$. Three cycles were performed per measurement. Thermogravimetric analyses (TGA) were performed in a TGA Q500 from TA with temperature ranging between room temperature and $600 \text{ }^\circ\text{C}$ with a heating rate at $10 \text{ }^\circ\text{C min}^{-1}$. The measurement was conducted in a nitrogen environment using a platinum pan. The optical micrographs were

recorded on a Leica DM2700 M polarized optical microscope equipped with a Leica MC170 HD camera. Electron micrographs were recorded using a Quanta FEG 3D SEM in secondary electron mode, with an accelerating voltage of 5 kV. Finally, Raman spectra were recorded on a Bruker SENTERRA dispersive Raman microscope. A confocal line scan was measured at the center of the microstructure, to a thermally polymerized film, and to a drop of the LC-photoresist using a 785 nm laser (70 mW s^{-1}), $100\times$ objective. The spectrum is the average of 50 measurements, each having an integration time of 1s.

LC-photoresist Characterization

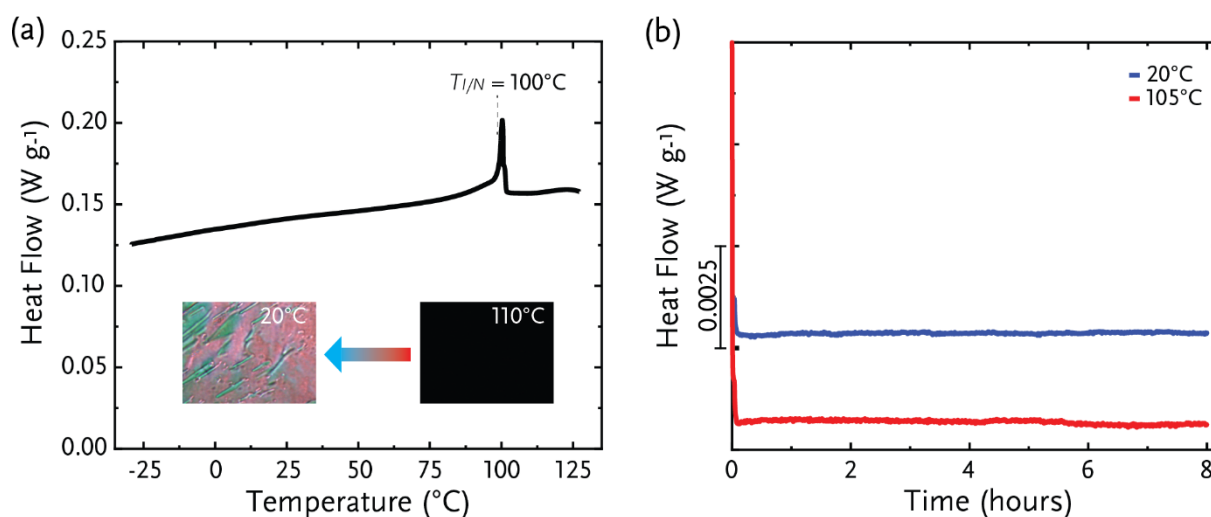


Figure S1. (a) DSC traces of a cooling cycle from the LC-photoresist, exotherm up. Inset: crossed polarized micrographs at 20°C depicting the nematic phase, and at 100° , showing the isotropic phase. (b) Isothermal measurements at 20°C and 105°C for 8h after cooling from 130°C .

Liquid Crystalline Network Characterization

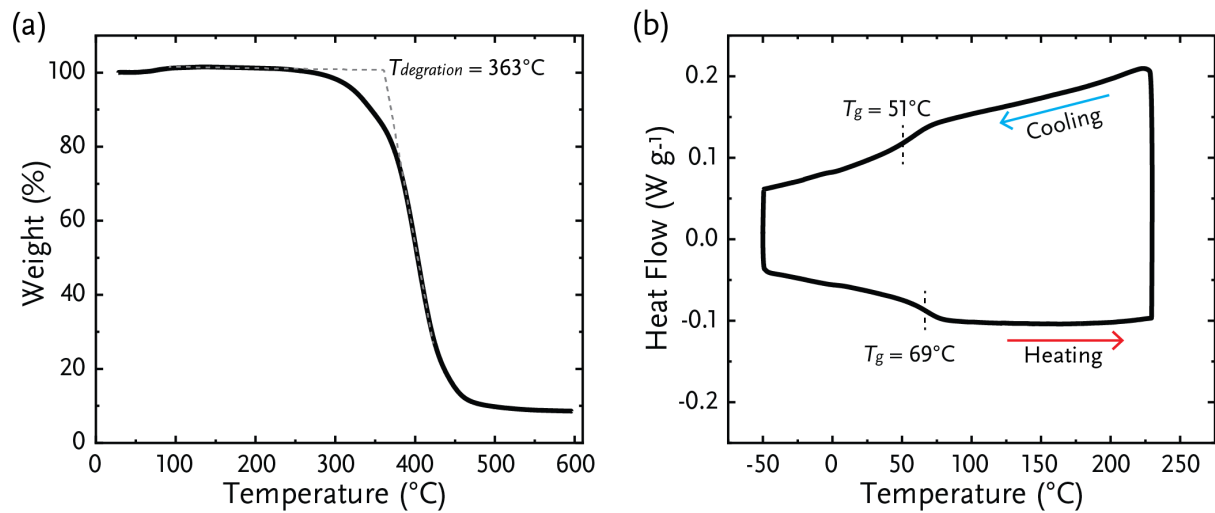


Figure S2. (a) TGA and (b) DSC traces of a uniaxially aligned polymer film made by photopolymerization of the LC-photoresist described in this work, exotherm up.

Computer Aided Designs

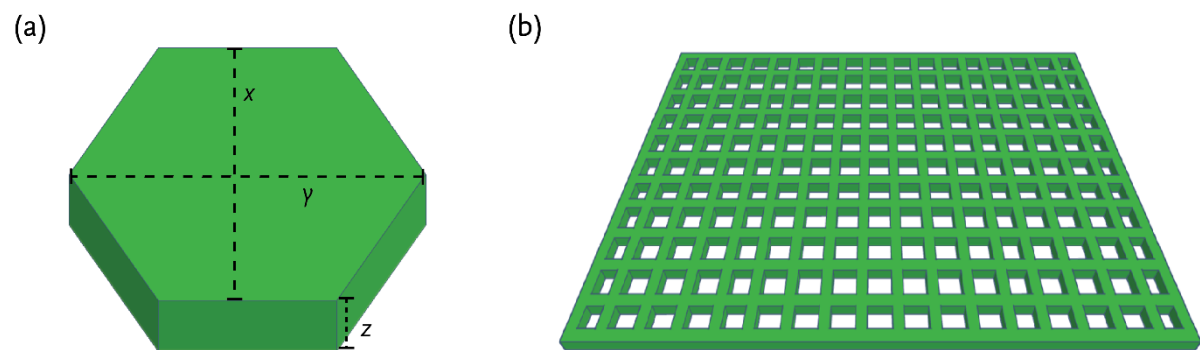


Figure S3. Computer aided design (CAD) of (a) a hexagonal plate and (b) a grid structure.

Dimension Characterization of Hexagonal Plates Fabricated in Different Fashions

Table 1. Dimensions of the different edges of hexagonal plates ($9\ \mu\text{m} \times 9\ \mu\text{m} \times 4\ \mu\text{m}$) fabricated using a rectilinear path that is shifted 0° , 45° , or 90° with respect of the alignment direction in the cell. Measurements were done at $20\ ^\circ\text{C}$. Error bars represent standard deviations for $N=4$ measurements.

Laser writing path direction with respect to the alignment	side x (μm)	side y (μm)	side z (μm)
0°	8.2 ± 0.1	8.5 ± 0.2	3.6 ± 0.1
45°	8.1 ± 0.2	8.7 ± 0.3	3.7 ± 0.3
90°	8.3 ± 0.3	8.8 ± 0.1	3.7 ± 0.1

Confocal Raman Spectroscopy

The verification of the complete two-photon polymerization of the microstructures was performed *via* confocal Raman spectroscopy, **Figure S4**. The spectrum of a microstructure was compared with the one of the LC-photoresist and a completely polymerized film, acting as a reference sample. The stretching of the C=C double bond of the acrylate group shows a strong peak at 1635 cm^{-1} and a medium peak at 1725 cm^{-1} , as seen in the spectrum of the LC-photoresist. The disappearance of these peaks indicates the reaction of the acrylate groups. These peaks disappear in either the spectra of the film or of the microstructure, indicating in both cases a successful polymerization of the monomers. Furthermore, the peak at 1735 cm^{-1} , characteristic to the vibration of the C=O from the acrylate is shifted to lower wavenumbers in the polymer samples (film and structure) indicating a change off its most near environment, further confirming the reaction of the acrylate groups.

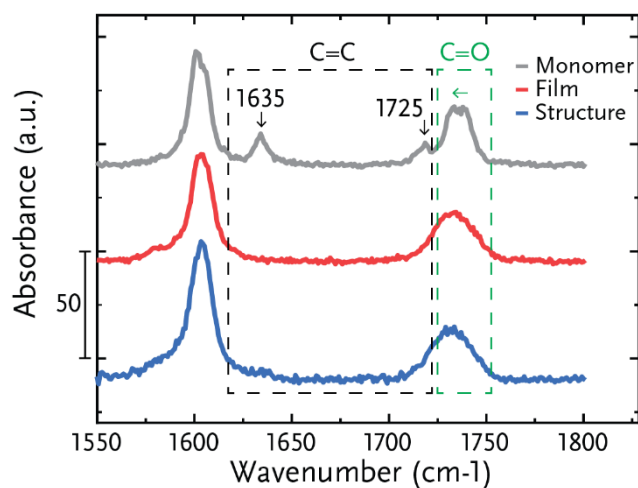


Figure S4. Confocal Raman spectroscopy of the LC-photoresist (or monomers), a fully polymerized film, and of a TPP-fabricated microstructure.